Biomass Conversion and Biorefinery
https://doi.org/10.1007/s13399-022-02865-8

ORIGINAL ARTICLE

Agricultural Pea Waste as a Low-Cost Pollutant Biosorbent for Methylene Blue Removal: Adsorption Kinetics, Isotherm And Thermodynamic Studies

Mathew C. Holliday[1,2] · Daniel R. Parsons[2] · Sharif H. Zein[1]

Received: 23 February 2022 / Revised: 9 May 2022 / Accepted: 23 May 2022

Abstract
Biosorbents are an alternative pollutant adsorbent, usually sourced from waste biomass and requiring little to no treatment. This makes them cheaper than conventional adsorbents. In this paper, green pea (*Pisum sativum)* haulm was used as a biosorbent for the adsorption of methylene blue dye. The potential application of pea haulm as a biosorbent has not been investigated before. Characterisation using scanning electron microscopy, infrared spectroscopy and thermal gravitational analysis showed the surface to be coarse, detected functional groups important for adsorption and identified the composition of key biomass components. The effects of particle size, contact time, agitation, dosage, solution pH, temperature and initial dye concentration on the removal of MB by pea haulm were investigated. Using the data from these studies, the best fitting kinetic and isotherm models were found and the thermodynamic properties were identified. The maximum theoretical adsorption capacity was 167 mg/g, which was relatively high compared to other recent biosorbent studies. The pseudo-second-order adsorption kinetic and Freundlich adsorption isotherm models were the best fitting models. The biosorption process was exothermic and spontaneous at low temperatures. It was concluded that pea haulm was an effective adsorbent of methylene blue and could perhaps find application in wastewater treatment.

Keywords Biosorption · Agricultural waste · Low-cost adsorbent · Methylene blue adsorption · Adsorption isotherms · Adsorption kinetics

1 Introduction

Textile pollution is a major contributor to water pollution. Coloured dyes are used in many industries such as textiles, paper, cosmetics, printing, food processing, leather, wool, and plastics [1–3]. They also consume large amounts of water, often resulting in significant effluent. It is estimated that 20% of clean water is polluted by the dyeing and finishing industry [4]. A large component of textile effluent is the unfixed dye. On average, about 10 -15% of unfixed dyes are released into water bodies after processing [5]. Basic dyes can be as little as 2%, whereas more reactive dyes can be as high as 50% [6]. In 2012, it was estimated that 200 billion litres of textile effluent were produced annually [7]. This pollution is mostly concentrated in newly industrialised countries, which saw rapid industrialisation but lacked pollution management. In 2017, It was estimated that 70% of groundwater was polluted in India and 90% in China; both have significant textile industries [5, 8].

Dye pollution is an environmental and health issue. It causes chemical and biological changes in polluted water bodies. Pollutants consume dissolved oxygen, causing aquatic animals to asphyxiate. Colour changes in the water prevent light from penetrating, resulting in the plants dying [3]. Even small amounts (less than 1 ppm) of some dyes are visible in the water [9]. This can cause entire underwater ecosystems and those that depend on them to perish. Most dyes are carcinogenic, mutagenic and can cause severe health hazards [10]. This can be deadly to animals and humans who rely on the water.

✉ Sharif H. Zein
s.h.zein@hull.ac.uk

[1] Department of Chemical Engineering, Faculty of Science and Engineering, University of Hull, Kingston Upon Hull, Hull HU6 7RX, UK

[2] Energy and Environment Institute, University of Hull, Kingston Upon Hull, Hull HU6 7RX, UK

Published online: 31 May 2022

There are many dyes available with different structures and properties. Dyes are hard to degrade because they are resistant to biodegradation, light, oxidising agents, biological activity, ozone and aerobic digestion and have high stability [10–13].

Unfixed dues must be removed from the effluent before it is released. A popular and effective method is the adsorption of the dissolved dye molecules using an adsorbent, and the most commonly used is activated carbon. However, it is expensive and demanding to produce, newly industrialised countries may not have the funding and infrastructure. Biosorbents are a cheaper and highly available alternative. They are cheaper because the only processing steps are washing and milling. A disadvantage is their smaller adsorption capacity, and the heterogeneous nature of plant matter leads to variation. This alternative adsorbent would be ideal in areas with high water pollution but no access to activated carbon.

There has been much interest in biosorbents over the decades, and they continue to be investigated due to different biomass yielding different results. Some impressive examples with high adsorption capacities are knotgrass, brewer's spent grain, fungi, berry seeds and soybean hulls [14–18]. To avoid unnecessary shipping, different biomass needs to be tested to see which local sources are appropriate for industrial sites. In this project, agricultural pea waste (haulm) from Yorkshire, England, was used.

The green pea (*Pisum sativum)* was used in this project, specifically the haulm. Pea haulm has not been investigated as a biosorbent before. Generally, vegetables will generate 30% (w/w) waste during harvesting and processing [19]. The waste biomass is often used to fertilise the soil or baled up to feed animals, but there is more than enough waste biomass to achieve this [20]. Green peas are part of the lignocellulosic family, the most abundant source of solid waste globally, comprising more than 60% of plant biomass produced by photosynthesis [21].

A commonly used dye in adsorption experiments is methylene blue (MB), a heterocyclic aromatic compound. It has the chemical formula $C_{16}H_{18}ClN_3S$, a molecular weight of 319.9 g/mole and a λmax of 665 nm. MB is a cationic dye, which is presumed to have the highest toxicity [22, 23]. MB can burn eyes, leading to permanent injury in humans and animals; when inhaled, it can cause breathing problems; when ingested, it can burn the mouth, cause nausea, vomiting, gastritis, profuse sweating, confusion, micturition and methemoglobinemia [24]. MB is primarily used in the acrylic, silk, nylon and wool dyeing industries [22]. The existence of an aromatic ring in the dye structures makes them highly toxic and mutagenic for human beings and aquatic life [25]. MB has a pronounced cationic feature in the amino group [15]. This suggests better adsorption in high pH. The structure of MB can be seen in Fig. 1.

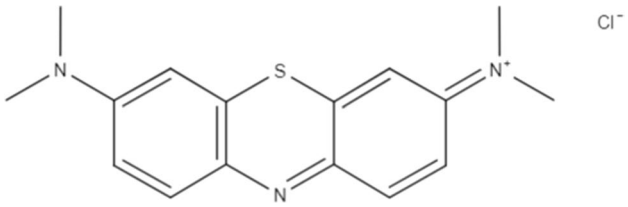

Fig. 1 Structure of methylene blue

This paper aims to answer whether waste pea haulm would make an effective biosorbent with an application in wastewater treatment and what variables affect adsorption. Waste pea haulm has not been investigated as a biosorbent before but offers an abundant supply of material. To answer this, the effects of particle size, contact time, agitation, dosage, solution pH, temperature, and initial dye concentration on MB removal by pea haulm were investigated. The results were used to fit theoretical kinetic and isotherm models to the adsorption process and determine the thermodynamic properties.

2 Materials and methods

2.1 Materials and Equipment

Pea waste was collected from farms in The Yorkshire region, England. It was washed, dried, and stored at 60 °C. It was milled using a Luvele Power-Plus 2200 W commercial blender and Waldner household mill lady to a fine powder. The powder was sieved by hand using Verder Scientific test sieves of various aperture. MB was bought from Sigma-Aldrich and used as received by dissolving in a deionised water solution. The dye mixtures were heated and agitated in a Stuart shaking incubator SI500. The mixtures were filtered using Whatman Grade 1 filter papers. The concentration of the dye was found using ultraviolet–visible spectroscopy (UV–Vis) spectroscopy, using a Jenway 7310 spectrophotometer, using a wavelength of 665 nm. pH was altered using citric acid and sodium hydroxide bought from Sigma-Aldrich. Solutions with a pH of 2 and 12 were made and diluted as required and tested using pH test strips.

The milled pea haulm was analysed using scanning electron microscopy (SEM) with energy-dispersive X-ray spectroscopy (EDX) using a TM4000plus tabletop microscope. Fourier transformed infrared analysis (FTIR) was performed using a Nicolet iS5 FTIR Spectrometer. A spectrum range of 525–4000 cm^{-1} was used with a resolution of 4 cm^{-1}. Thermo-gravimetric analysis (TGA) was performed using a TGA 4000 unit by PerkinElmer. A temperature range of 50–800 °C was used with a thermal gradient of 20 °C/min under nitrogen. The pH of zero charge was

found by mixing 0.15 g of biomass with 0.01 mol/L NaCl and dissolved in 100 mL of deionised water and then altering the pH to 2, 4.5, 7, 9.5 and 12 using 0.1 mol/L HCl and NaOH [26]. After 24 h, the new pH was recorded. The pH was measured using Preciva PH Meter.

2.2 Methods

Batch adsorption was chosen because of availability, facility of operation and reliability, other methods such as oxidation and flocculation produce mud, and membrane separation requires high pressures [27]. The following adsorption experiments are based on the methodology of previous studies on the adsorption of MB using biosorbents [14, 15, 18, 28, 29]. Like these other studies, the effects of dosage, solution pH, residence time, solution temperature, initial dye concentration, particle size and agitation were investigated. However, this paper focuses on the biosorption of MB using pea haulm, of which there have been no previous studies. There have been studies on pea peels, but these are different waste products [2, 22]. Every experimental run was repeated three times to avoid inaccuracy.

2.2.1 Methylene blue calibration curve

A calibration curve was required to understand the relationship between UV light absorbance and MB concentration. Known MB concentrations were analysed using UV–Vis at an absorbance wavelength of 665 nm. A line graph was created using MB concentration against the UV absorbance value. This curve could be used to translate UV–Vis absorbance to MB concentration.

A calibration curve was also required when filtering the pea haulm out of the dye mixtures. This is because some of the dye was absorbed by the filter paper during filtration. Known MB concentrations were filtered, and then, the filtrate was analysed using UV–Vis. This would reveal how much of the dye was lost to the filter papers. A line chart of pre-filter concentrations against post-filter concentrations was made.

2.2.2 Effect of particle size on biosorption

Pea haulm was milled and then sieved to size ranges of 500–200 µm, 200–50 µm and < 50 µm. 0.01 g of the different sized biomass was added to a 20 mL of 50 mg/L MB solution (giving a dosage of 0.5 g/L). The solution was agitated at 120 rpm and heated to 30 °C for 4 h. The solution was filtered of solids, diluted and analysed using UV–Vis.

2.2.3 Effect of agitation rpm on biosorption

0.01 g of < 50 µm biomass was added to 20 mL of 50 mg/L MB solution. The solution was heated to 30 °C and agitated at 0, 60, 120 and 180 rpm for 4 h. The solution was then filtered, diluted, and analysed using UV–Vis.

2.2.4 Effect of contact time on biosorption

0.01 g of < 50 µm biomass was added to 20 mL of 50 mg/L MB solution. The solution was heated to 30 °C and agitated at 120 rpm. Solutions were filtered after a period ranging from 0.5 to 1440 min. For 0.5 min, the pea haulm was added, gently shaken and then immediately filtered. The solutions were then filtered, diluted, and analysed using UV–Vis to find the removal of MB.

2.2.5 Effect of haulm dosage on biosorption

0.01, 0.05 and 0.1 g of < 50 µm biomass was added to 20 mL of 50 mg/L MB solution (0.5, 2.5 and 5 g/L, respectively). The solution was heated to 30 °C and agitated at 120 rpm. After 4 h, the solution was filtered, diluted, and analysed using UV–Vis to find the removal of MB.

2.2.6 Effect of solution pH on biosorption

0.01 g of < 50 µm biomass was added to 20 mL of 50 mg/L MB solution. The solution pH was altered to 4.85, 7, 8, 10 and 12 using a citric acid or sodium hydroxide solution instead of pure deionised water. The solution was heated to 30 °C and agitated at 120 rpm. After 24 h, the solution was filtered, diluted, and analysed using UV–Vis to find the removal of MB.

2.2.7 Effect of initial concentration and temperature on biosorption

0.01 g of < 50 µm biomass was added to 20 mL of 25, 50, 75 and 100 mg/L solutions. The solutions were heated to 30 °C and agitated at 120 rpm. After 24 h, the solution was filtered, diluted, and analysed using UV–Vis to find the amount of MB removed. This was repeated at 45 and 60 °C.

2.2.8 Adsorption kinetics

The pseudo-first- and second-order kinetic models were used in this study. The nonlinearised and linearised pseudo-first-order (PFO) kinetic model can be seen in Eqs. 1 and 2, respectively [30].

$$q_t = q_e(1 - e^{-k_1 t}) \tag{1}$$

$$\ln(q_e - q_t) = \ln(q_e) - k_1 t \tag{2}$$

where q_t is the amount of MB adsorbed (mg/g) at time t (min), q_e is the amount of MB adsorbed (mg/g) at equilibrium, and k_1 is the PFO rate constant of the adsorption (min^{-1}). For pseudo-second-order (PSO) kinetics, the nonlinearised and linearised PSO kinetic model can be seen in Eqs. 3 and 4, respectively [31].

$$q_t = \frac{k_2 {q_e}^2 t}{1 + k_2 q_e t} \tag{3}$$

$$\frac{t}{q_t} = \frac{1}{k_2 {q_e}^2} + \frac{t}{q_e} \tag{4}$$

k_2 is the PSO rate constant of the adsorption processes (g mg^{-1} min^{-1}).

2.2.9 Adsorption isotherms

The Langmuir, Freundlich, Temkin & Pyzhev (TP) and Dubinin & Radushkevich (DR) isotherm models were used in this study. The nonlinearised and linearised Langmuir isotherm equation is seen in Eqs. 5 and 6, respectively [32]:

$$q_e = \frac{Q_{max} k_L C_e}{1 + k_L C_e} \tag{5}$$

$$\frac{1}{q_e} = \frac{1}{Q_{max} k_L C_e} + \frac{1}{Q_{max}} \tag{6}$$

C_e is the concentration of MB at equilibrium (mg/L), Q_{max} is the maximum amount of adsorbate adsorbed at equilibrium when the adsorbent is saturated (mg/g), and k_L is the Langmuir isotherm constant which is related to the affinity of the binding sites and the adsorption free energy (L/mg). The separation factor (R_L) was also found using the Langmuir isotherm constant, seen in Eq. 7 [33].C_0 is the initial MB concentration (mg/L).

$$R_L = \frac{1}{1 + K_L C_0} \tag{7}$$

The nonlinearised and linearised versions of the Freundlich isotherm can be seen in Eqs. 8 and 9, respectively [34]:

$$q_e = K_F (C_e)^{1/N} \tag{8}$$

$$\ln(q_e) = \ln(K_F) + \frac{1}{n}\ln(C_e) \tag{9}$$

K_F is the Freundlich constant related to the adsorption capacity ((mg/g) $(L/mg)^{1/n}$), and n is an empirical parameter associated with the intensity of adsorption and indicates heterogeneity. The nonlinearised and linearised equation of the TP isotherm can be seen in Eqs. 10 and 11, respectively [35]:

$$q_e = \frac{RT}{B}\ln(K_T C_e) \tag{10}$$

$$q_e = \frac{RT}{B}\ln(K_T) + \frac{RT}{B}\ln(C_e) \tag{11}$$

R is the universal gas constant (8.314 J/(K·mol)), T is the absolute temperature in Kelvin, B is the TP constant related to the heat of sorption (J/mole), and K_T is the equilibrium constant corresponding to the maximum binding energy (L/mg). The nonlinearised and linearised equation of the DR isotherm can be seen in Eqs. 12 and 13, respectively [36]:

$$q_e = Q_m e^{-K_D \varepsilon^2} \tag{12}$$

$$\ln(q_e) = \ln(Q_m) - K_D \varepsilon^2 \tag{13}$$

Q_m is the maximum adsorption capacity (mg/g), K_D is the DR Isotherm constant (mol^2/kJ^2), and ε is the Polanyi potential. The Polanyi potential is calculated using Eq. 14 [36]:

$$\varepsilon = RT\ln\left(1 + \frac{1}{C_e}\right) \tag{14}$$

The mean free energy of adsorption can be found using the DR Isotherm constant and Eq. 15.

$$E = \frac{1}{\sqrt{(2K_D)}} \tag{15}$$

E is the mean free energy of adsorption, which is the free energy charge when one mole of ion is transferred from infinity in the solution to the surface of the sorbent (kJ/mole).

2.2.10 Adsorption thermodynamics

To find the thermodynamic properties of enthalpy, entropy and Gibbs free energy, the following equations were used. The formula to find the apparent equilibrium constant, K_c can be seen in Eq. 16:

$$K_c = \frac{C_{Ads,e}}{C_e} \tag{16}$$

$C_{Ads,e}$ is the concentration of MB adsorbed by the adsorbent at equilibrium (mg/L). The Gibbs free energy can be calculated using the equilibrium constant, seen in Eq. 17:

$$\Delta G = -RT\ln\left(K_c\right) \tag{17}$$

ΔG is the Gibbs free energy change (J/mol). The enthalpy and entropy of the MB adsorption can be found Using the Gibbs free energy and temperature, seen in Eq. 18:

$$\Delta G = \Delta H - T\Delta S \tag{18}$$

ΔH is the enthalpy change (J/mol), and ΔS is the entropy change (J/mol K).

2.2.11 Model validity

The best-fitting models cannot be found using only the correlation coefficient (R^2) and require other forms of model validity evaluation [27]. The goodness of fit was evaluated using the sum of the squared estimate of errors (SSE) and the root-mean-square error (RMSE). These methods of evaluation have been used in similar adsorption studies [11, 27, 37]. SSE was found using Eq. 19:

$$SSE = \sum \left(q_{exp} - q_{cal}\right)^2 \tag{19}$$

where q_{exp} is the adsorption derived from experimental and q_{cal} is the calculated adsorption from the kinetic or isotherm study. RMSE was found using Eq. 20:

$$RMSE = \sqrt{\frac{SSE}{N}} \tag{20}$$

where N is the number of data points. The best fitting model will have an R^2 value that is closest to 1.0 and the lowest SEE and RMSE values.

3 Results and discussion

3.1 Characterisation

3.1.1 SEM and EDX

SEM images were taken of the pea haulm milled to < 50 µm. The aim was to find any porous structure that may suggest a high adsorption capacity. The images can be seen in Figs. 2A and B.

It can be seen in Figs. 2A and B that the surface appears very coarse and heterogeneous. The heterogeneous nature of raw biomass causes inconsistencies in the adsorption results. It contains many cracks and crevices but also rigid and ordered fibres despite being finely milled, which is characteristic of a lignocellulosic structure [15]. The particles are all less than 50 microns on at least one side. A course surface suggests many folds and undulations, increasing surface area. The increased surface area can increase access to surface adsorption sites assisting adsorption. This relationship is explored in Sect. 3.2, the effect of particle size, where the surface-to-volume ratio changes. The material likely does not have micro- and nanostructures due to the lack of treatment. This will mean it has low porosity. Due to the low surface area and

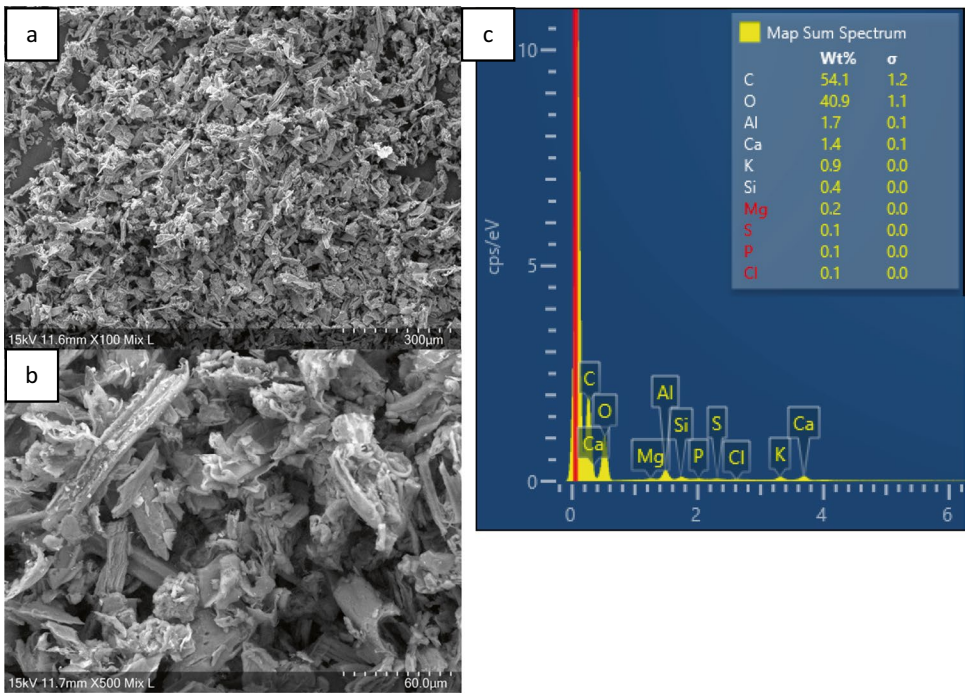

Fig. 2 **a**) Magnified pea haulm × 100 magnification, **b**) magnified image × 500 magnification, **c**) EDX spectra of pea haulm

porosity, it can be assumed that pea haulm uses chemical mechanisms to adsorb MB rather than physical. It highlights the importance of the surface chemistry of the biosorbent. In another study, SEM images after adsorption showed a smooth surface and reduced porosity due to the impregnation of MB onto the surface [14].

From the SEM images, an EDX scan was taken. The spectrum can be seen in Fig. 2C. This revealed the elemental composition of the material surface. The surface was 54.1% carbon, 40.9% oxygen and the rest other inorganics. As expected from biomass, the pea waste was found to be about half carbon and half oxygen. There are a few trace elements that are normal for plant material. No nitrogen was identified. In the EDX spectrum of other biomass, a small peak of nitrogen can be seen between the large peaks of carbon and oxygen [14, 18, 28]. It could be assumed that the large carbon and oxygen peaks may have overlapped a small peak of nitrogen. In another study, EDX spectra after adsorption showed an increased amount of nitrogen and silica, showing MB had been adsorbed to the surface [14].

3.1.2 FTIR

Pea haulm was analysed using FTIR. FTIR was used to find important functional groups that would help adsorption and suggest a high adsorption capacity. The annotated spectrum can be seen in Figs. 3A and B.

The spectrum should show groups found in cellulose, hemicellulose and lignin. To identify the functional groups, the spectrum was compared with those from literature. The wide trough at 3326 cm^{-1} is likely OH groups associated with cellulose and lignin [14, 15]. The small troughs at 2933 cm^{-1}, 2888 cm^{-1} and 2850 cm^{-1} are likely aliphatic C-H groups associated with lignin [14, 15]. The trough at 1729 cm^{-1} is likely a C = O group of carboxylic acids or esters, associated with hemicellulose [14, 15]. The trough at 1612 cm^{-1} is likely akene C = C groups or C = O/N–H groups of amide I [15–17]. The trough at 1513 cm^{-1} is likely N–H/C-N groups of amide II [15]. The trough at 1421 cm^{-1} is likely aromatic C = C groups [14]. The trough at 1366 cm^{-1} is likely methyl C-H groups [16, 17]. The trough at 1316 cm^{-1} is likely an aromatic ring group [18]. The troughs at 1230 cm^{-1} and 1021 cm^{-1} are likely C-O groups of carboxylic acids, present in lignin [15, 18]. The trough at 1148 cm^{-1} is likely the aromatic rings of lignin or C-O groups [16, 18]. The trough at 893 cm^{-1} is likely C-H linkages in cellulose [15, 17, 18]. There is evidence of hydroxyl, carbonyl, carboxyl, ester and aromatic groups, which are important for adsorption and explained in Sect. 3.1.5 [26].

3.1.3 TGA

TGA was used to estimate the composition of biomass components. Hemicellulose degrades at 220–315 °C, cellulose degrades at 315–400 °C, and lignin degrades over 160–900 °C [38]. The TGA data are seen in Fig. 4. The dotted lines are the degradation temperatures of the main components in biomass.

The TGA curve can be broken into different mass losses. This can be used to give a rough estimation of the composition. The weight loss before 160 °C was assumed to be volatiles such as moisture, and it can be assumed that 3% of the biomass is volatiles. It was assumed that lignin is lost at a rate of 0.033%/°C based on the mass lost between 160–220 °C and 400–800 °C, meaning 22% is lignin. Once lignin is subtracted, there remains 18% hemicellulose, 37% cellulose and 20% ash. The weight continued to decrease beyond 800 °C, so ash content is likely much lower and lignin higher. The composition is represented in Fig. 5.

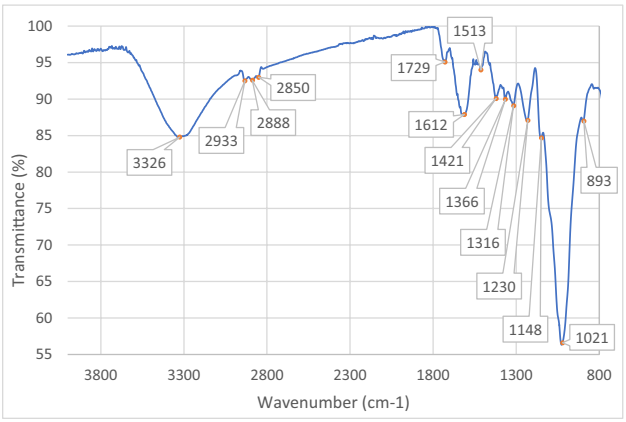

Fig. 3 Pea haulm FTIR spectrum, **a**) spectrum between 3700–2700 cm^{-1}, **b**) spectrum between 1800–800 cm^{-1}

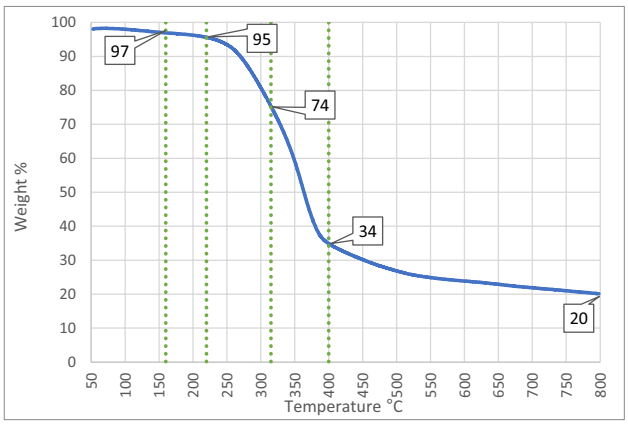

Fig. 4 TGA of pea haulm, points at 160, 220, 315 and 400 °C, marking the key thermal degradation points of hemicellulose, cellulose and lignin and the mass loss (wt%) at these points

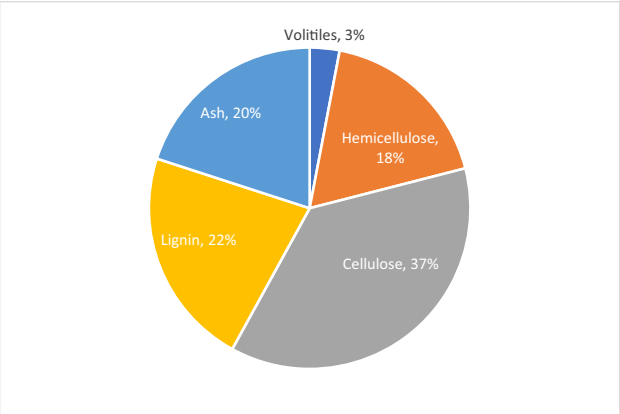

Fig. 5 Pea haulm composition

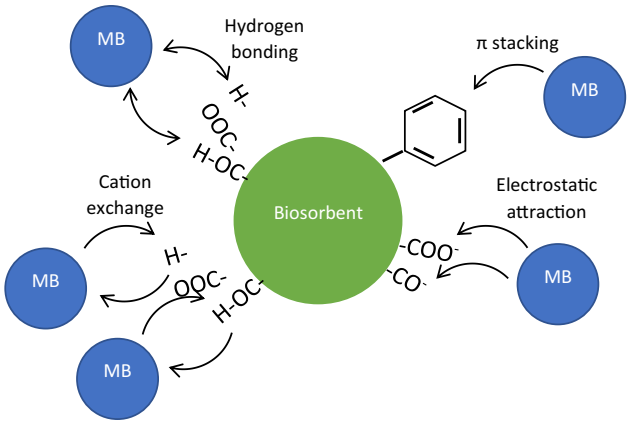

Fig. 7 Possible methylene blue adsorption mechanisms

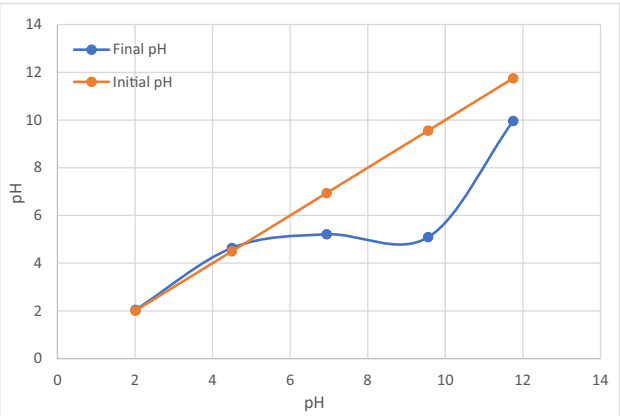

Fig. 6 PH of zero charge

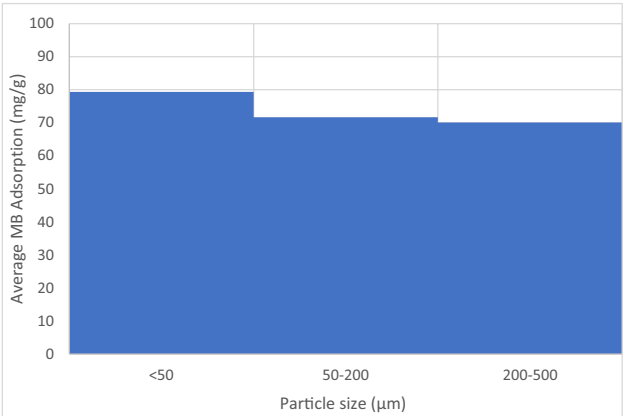

Fig. 8 Effect of particle size on methylene blue adsorption

Generally, pea peels contain 75% cellulose and hemicellulose [21]. In this study cellulose and hemicellulose make up only 55%. The increased lignin content is likely due to the rigidity required in the stalks and vines of the pea plant.

3.1.4 PH of zero charge

The zero-point charge indicates the external surface charge of the material [18]. The intersection of the initial and final pH corresponds to the pH of zero charge (PZC). This graph can be seen in Fig. 6.

The $pH_{(PHZ)}$ was about 4.75. This means that when pH is lower than 4.75, the biosorbent surface is positively charged and when the pH is above 4.75, the surface of pea haulm is negatively charged [26]. Since MB is cationic, it is expected that a negatively charged surface will promote adsorption.

3.1.5 Adsorption mechanism

Cellulose, hemicellulose and lignin contain benzene rings, hydroxyl and carboxyl groups. These groups were identified in the FTIR characterisation. These groups will interact differently with the structure of MB, causing the MB to adhere to the surface of the biosorbent. The interactions have been described in other works [15, 18]. Interactions include the π stacking between benzene rings in MB and the biosorbent [28]. Another interaction is the net positive charge of MB, leading to electrostatic attraction to negative groups on the biosorbent. Another interaction is hydrogen bonding between the biosorbent and the MB. A final interaction is cation exchange between the MB molecule and the biosorbent. This means biosorbents with a large amount of benzene, hydroxyl and carboxyl groups will likely be better adsorbents. Figure 7 illustrates these possible adsorption mechanisms.

3.2 Effect of particle size on biosorption

Particle sizes of 500–200, 200–50 and < 50 µm were used to adsorb MB. The results can be seen in Fig. 8.

It is shown that small particle size is most effective for adsorption. Adsorption occurs on the surface of the adsorbent. A smaller particle size increases the surface to volume ratio, increasing the available adsorption sites. Due to the success of the particles below 50 µm, this size was used in the other investigations.

Particle size has been investigated in other studies [28]. They used size of ≤ 36, ≤ 160, and ≤ 425 µm. They also found that decreasing particle size increased adsorption. In a different study, they used sizes of 425, 600 and 850 µm [39]. They found that the two smaller sizes were not significantly different, but 850 µm had a lower adsorption capacity. This suggests that the benefit of small particle sizes may stop at a certain point.

A lot of energy is required for size reduction, and handling the material becomes difficult. A finer material will become suspended easily, potentially leading to a loss of material. The particles can cause respiratory problems or even cause dust explosions. Particles of less than 10 microns can make their way deep into the lungs [40]. Milling produces heat that can alter the biomass. The heat from different milling processes can denature proteins, reduce amino acids, and reduce saturated fatty acids in wheat flour [41]. This could negatively affect the biosorbent's effectiveness.

3.3 Effect of agitation rpm on biosorption

The effects of agitation on biosorption were tested using an rpm of 0, 60, 120 and 180. The results can be seen in Fig. 9.

It was found that agitation of 120 rpm had the most favourable effect on MB adsorption. It was also found that 0, 60 and 180 rpm had an equal effect. One possible reason for this could be the small particle size and low dosage. It could be assumed that the biosorbent particles were evenly dispersed throughout the dye mixture and small enough to avoid overlapping and aggregation. Therefore, a lack of agitation would not be entirely detrimental. The reason the adsorption decreases at 180 rpm may be because of a slight centrifugal effect, separating the biosorbent from the dye. With a larger particle size and dosage, the effect of agitation would likely be more significant.

The agitation has been investigated in another study [29]. They used an rpm of 50–150 with 100 mL of 5 mg/L MB solution and with a dosage of 2.5 g. No particle size was recorded. They used a lower dye concentration and higher dosage, but they also noted agitation had little effect on adsorption. They concluded that the slight increase in biosorption was caused by increased diffusion and more MB molecules at the liquid–solid boundary layer. They also wrote that this would decrease the thickness of the liquid boundary layer. They speculated that the agitation may have also caused the biosorbent to fragments, further increasing its surface area.

Increasing agitation will help the transportation and mass transfer of dye molecules through the boundary layer, increasing surface interactions. These increased interactions should lead to a faster equilibrium and increased adsorption. With no agitation, the solids will settle to the bottom of the solution, decreasing the available adsorption sites. An alternative scenario is that the biosorbent may float, unable to break the surface tension of the solution.

3.4 Effect of contact time on biosorption

The effect of contact time was investigated. A contact time of 0.5–1440 min was used. The results are displayed in Fig. 10.

It was found that MB adsorption increased as contact time was extended. This is because the mixture was yet to reach equilibrium, and not all the active adsorption sites were filled. Equilibrium was on average reached after about 4 h when the adsorption sites were fully saturated. The highest adsorption achieved experimentally in this investigation was 87 mg/g at 1440 min. Saturation occurs when the majority

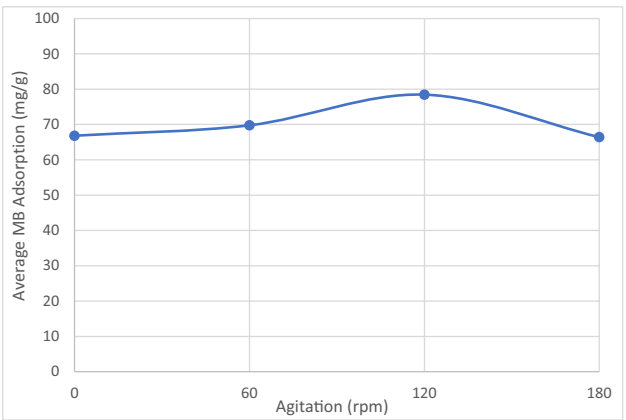

Fig. 9 Effect of agitation on methylene blue adsorption

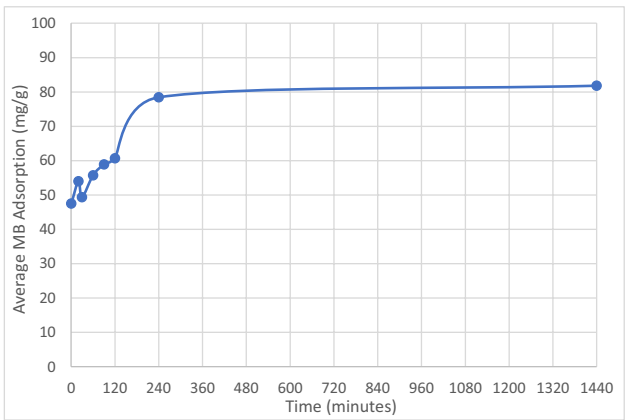

Fig. 10 Effect of contact time on methylene blue adsorption

of sites are filled and the negatively charged MB molecules will repulse the remaining MB molecules on the biosorbent surface. It is important to know when equilibrium is reached because a longer processing time will increase production costs.

It can be seen that the biosorption process occurs almost immediately, suggesting a high affinity. Even when the biosorbent is added and then quickly removed after 30 s, 48% of the MB is removed. The average results varied significantly. This is likely due to the heterogeneous nature of the biosorbent. Biomass is made up of different components and is not uniform or consistent. This results in varied adsorption capacities making biosorbents unreliable.

3.5 Effect of haulm dosage on biosorption

The effect of adsorbent dosage on biosorption was investigated. A dosage of 0.5, 2.5 and 5 g/L was used. The results can be seen in Fig. 11, showing MB adsorption and removal simultaneously.

It can be seen in Fig. 11 that increasing the dosage increases the MB removal. This is because the number of available adsorption sites increases. This improvement will stop at higher dosages because the lack of dispersion causes adsorption sites to overlap and aggregate, reducing the surface area. The maximum experimental MB removal was 89%, using 0.1 g of biosorbent. When dosage increases, the adsorption decreases. This is because there are more unsaturated sites per mass of biosorbent, reducing the efficiency.

It is important to maximise the efficiency by adsorbing as much pollution using as little adsorbent as possible. In some scenarios, multiple passes using a low dosage may be preferable over a single pass using a larger dosage. This will take advantage of the higher adsorption capacity of lower dosages. A dosage of 0.01 g was used in the other investigations to maximise the adsorption value.

3.6 Effect of solution pH on biosorption

The effect of pH on MB adsorption was investigated. pH values of 4.85, 7, 8, 10 and 12 were used. Figure 12 shows how pH affected MB adsorption.

It can be seen that the adsorption capacity increases in alkaline conditions. The adsorption capacity increased significantly after a pH of 10. A pH lower than 7 resulted in a lower adsorption capacity. A pH lower than 4.85 resulted in low adsorption that the calibration curve could not accurately translate. The solution at low pH was visually darker, confirming this. This correlates with the pH of zero charge which was about 4.75. At pHs lower than 4.75, the surface will be positively charged and repel positively charged MB particles.

Most studies had similar results, with adsorption increasing with a higher pH and decreasing with a lower pH [14, 15, 17, 42]. MB is cationic and attracted to negative charges. In acidic conditions, the surface of the biosorbent will be positively charged. The negative charges from the carboxyl and hydroxyl groups are reduced by the high concentration of H^+ ions [14]. At a higher pH, The surface will be more negatively charged, increasing the electrostatic attraction between the biosorbent and pollutant. The carboxyl and hydroxyl groups will become completely deprotonated increasing the negative charge [15].

In some other studies, pH did not affect adsorption [18]. This is because the biosorbent surface was negative in all circumstances.

In some other studies, adsorption decreased with both an increase and decrease in pH [29]. They concluded that at a high pH the overwhelming negative charge resulted in the dye becoming deprotonated as well, causing the pollutant and adsorbent to repel each other [29]. However, they used

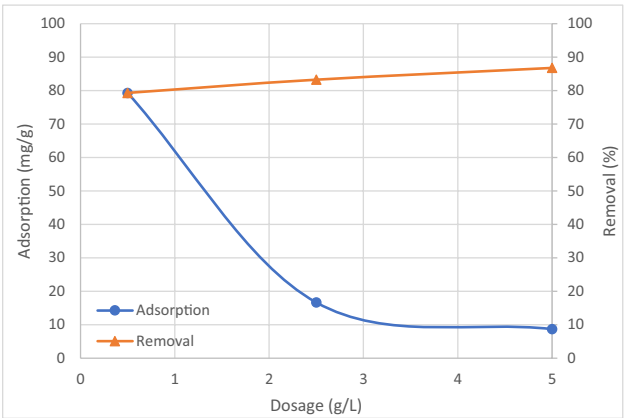

Fig. 11 Effect of biosorbent dosage on methylene blue adsorption and removal

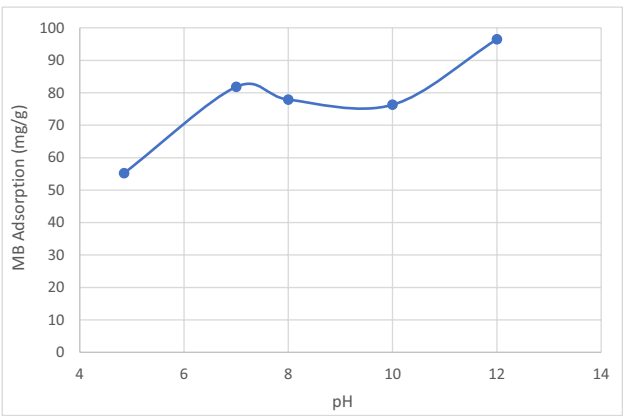

Fig. 12 Effect of solution pH on methylene blue adsorption

a very high dosage and very low MB concentration, which may have affected the outcome.

3.7 Effect of initial concentration on biosorption

The effect of the initial MB concentration on adsorption was investigated. Initial concentrations of 25, 50, 75 and 100 mg/L were used. Figure 13 shows how the initial concentration affected adsorption and removal.

It can be seen that the adsorption capacity increases with the initial MB concentration. This is because there are more MB molecules, increasing the chance of interactions with the surface of the adsorbent. The increase in interactions means it is more likely for previously unfilled adsorption sites to be filled. The adsorption capacity is likely to increase beyond 100 mg/L. However, higher concentrations were not investigated due to the increased dilution leading to a decrease in calibration curve accuracy. The adsorption capacity should stop increasing when the maximum adsorption capacity is reached. The maximum adsorption capacity is important because it is used to determine how effective the material is for adsorption. The highest adsorption capacity achieved experimentally was 153 mg/g at 100 mg/L. The maximum adsorption capacity can also be found theoretically using adsorption kinetics or isotherm models.

3.8 Effect of solution temperature on biosorption

The effect of temperature on biosorption was investigated. Temperatures of 30, 45 and 60 °C and initial MB concentrations of 25, 50, 75 and 100 mg/L were used. The results can be seen in Fig. 14.

It can be seen that a lower temperature is better for adsorption, so it can be assumed that the process is exothermic. This is because the state of adsorption has lower energy than the MB solution, resulting in a loss of energy. These results were used in the isotherm and thermodynamic study. Exothermic results were shown in similar studies [16, 18, 42]. It was suggested that the increased temperature might weaken the intermolecular bonds between the MB molecules and biosorbent [42].

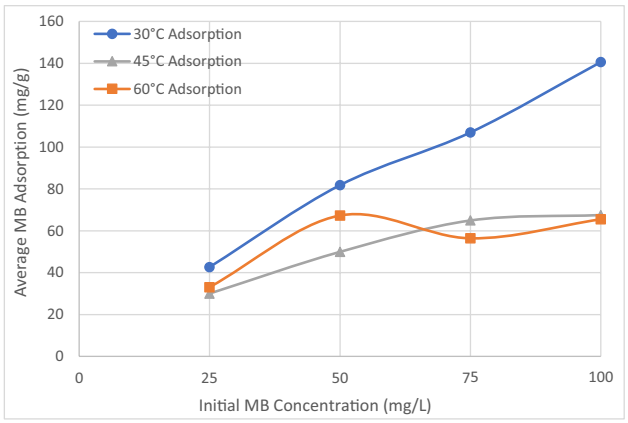

Fig. 14 Effect of solution temperature on methylene blue adsorption

It is important to know the effects of temperature on adsorption because applying heat to the mixture would use significant energy and cost money. Since the process is exothermic, it can be performed efficiently and safely at room temperature. It also means heating restrictions will not limit the dimensions of the filtration vessel.

3.9 Determination of adsorption kinetic model

The kinetic model is used to mathematically describe the adsorption mechanism of the dye molecules moving through the bulk solution to the biosorbent surface. The PFO and PSO kinetic models were used in this investigation.

For PFO kinetics, Eq. 2 was used to build a linear curve using the data from Fig. 10 and an axis of $ln(q_e\text{-}q_t)$ and t.

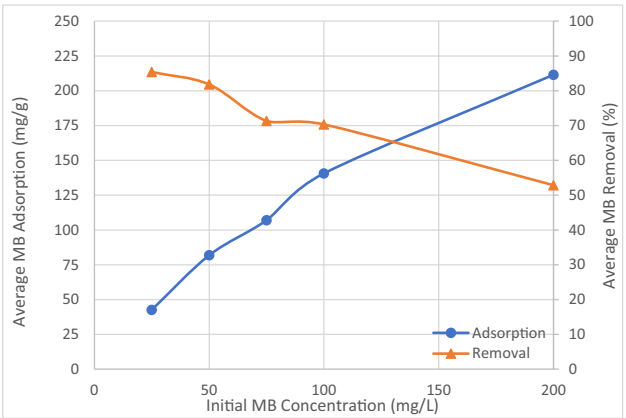

Fig. 13 Effect of initial MB concentration on methylene blue adsorption and removal

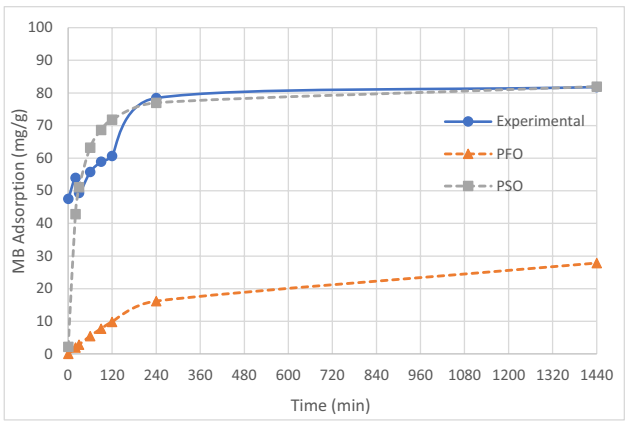

Fig. 15 Lagergren (1898) pseudo-first-order-linear kinetic model and Ho & McKay (1998) pseudo-second-order linear kinetic model plotted with experimental results

Table 1 Kinetic model parameters

Model	Parameter	Value
Pseudo-first-order	$q_{e(exp)}$(mg/g)	82
	$q_{e(cal)}$(mg/g)	28
	k_1(min^{-1})	0.0036
	R^2	0.9288
	SSE	21,651
	RMSE	49
Pseudo-second-order	$q_{e(cal)}$(mg/g)	83
	k_2(g mg^{-1} min^{-1})	0.000642
	R^2	0.9991
	SSE	2,461
	RMSE	16.5

This curve was used to find q_e, k_1 and R^2. These values were fitted into Eq. 1 and plotted in Fig. 15. For PSO kinetics, a linear curve can be made using Eq. 4 and the data in Fig. 10 using an axis of t/q_t and t. This curve was used to find q_e, k_2 and R^2. These values were fitted into Eq. 3 and plotted in Fig. 15.

The parameters of the kinetic models are summarised in Table 1. $q_{e(exp)}$ is the highest experimental adsorption achieved at 50 mg/L. $q_{e(cal)}$ is the theoretical adsorption capacity.

The PSO kinetic had a higher R^2 value and lower SSE and RMSE than the PFO kinetic model, and the calculated adsorption capacity was closer to the experimental adsorption capacity. This means the PSO kinetic model can be used to describe the process. Most biosorbents can be described using PSO kinetics.

3.10 Determination of isotherm adsorption model

An isotherm model can be used to describe mathematically the equilibrium between the dye concentration in the bulk solution and the dye adsorbed by the adsorbent. Different models use different assumptions. The Langmuir isotherm is one such model. It assumes the surface is uniform, adsorption energy is dispersed evenly, each adsorption site contains one adsorbed molecule, molecules do not interact, adsorption leads to a monolayer, and the process is irreversible [16, 28, 39]. These assumptions allow the monolayer capacity to be calculated. Equation 6 can be used to form a linear line using the data seen in Fig. 13 and using an axis of $1/q_e$ and $1/C_e$ to find the k_L, Q_{max} and R^2. The values were used in Eq. 5 and plotted on Fig. 16 with the experimental values for comparison. Since the process is exothermic, the 30 °C isotherm will be the focus of the investigation.

Using the Langmuir isotherm constant, the separation factor can be identified using Eq. 7. It identifies whether the adsorption process is favourable or not. The R_L value indicates whether the adsorption is unfavourable (RL > 1), linear (RL = 1), favourable (RL < 1) or irreversible (RL = 0). At 25 mg/L, the separation factor is 0.3; at 100 mg/L, the factor is 0.09; it can be assumed that the process is favourable between these concentrations.

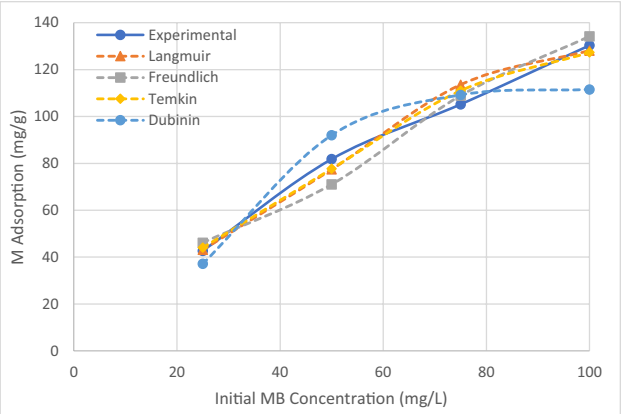

Fig. 16 Langmuir (1916) isotherm, Freundlich (1906) isotherm, Temkin & Pyzhev (1940) model and Dubinin & Radushkevich (1947) Isotherm with experimental results

The Freundlich model is another isotherm model. This isotherm is used when the process does not match the conditions of the Langmuir isotherm, such as heterogeneous surface and multi-layering [16]. Equation 9 can be used to form a linear line using the data seen in Fig. 13 with the axis $ln(C_e)$ and $ln(q_e)$ to find K_F, $1/n$ and R^2. The values are used in Eq. 8 and plotted in Fig. 16 with the experimental values for comparison.

The TP model is another adsorption isotherm model. It considers the effects of indirect interactions between the biosorbent and MB molecules, and it assumes there is a uniform distribution of binding energy [18]. Equation 11 can be used to form a linear line using the data seen in Fig. 13 with the axis $ln(C_e)$ and q_e to find K_T, B and R^2. The values were used in Eq. 10 and plotted in Fig. 16 with the experimental values for comparison.

The final isotherm model investigated is the DR model. It assumes a multilayer of molecules using Van der Waal forces and is important in describing the adsorption of vapours and gases [28]. Equations 13 and 14 can be used to create a curve using the data in Fig. 13, using the axis ε^2 and $ln(q_e)$ to find K_D, Q_m and R^2. The values are used in Eq. 12 and plotted in Fig. 16 with the experimental values for comparison.

The parameters for each model are summarised in Table 2.

All the models had a very high R^2 value. Although the Langmuir isotherm had the highest R^2 value, it had a higher SSE and RMSE value than TP. This shows the model cannot be determined by R^2 alone. The order of

Table 2 Isotherm parameters

Isotherm Model	Parameter	Value
	$Q_{max,exp}$ (mg/g)	153
Langmuir	Q_{max}(mg/g)	167
	K_L(L/mg)	0.095
	R_L	0.3–0.09
	R^2	0.993
	SSE	95
	RMSE	4.87
Freundlich	K_F((mg/g) (L/mg)$^{1/n}$)	25
	$1/n$	0.47
	R^2	0.96
	SSE	157
	RMSE	6.27
TP	K_T(L/mg)	0.9
	B (J/mole)	68
	R^2	0.9851
	SSE	62
	RMSE	3.94
DR	K_D(mol^2 kJ^{-2})	0.000003
	Q_m(mg/g)	113
	E (kJ/mole)	408
	R^2	0.9354
	SSE	504.68
	RMSE	11.23

the best-fitting model based on RMSE was TP > Langmuir > Freundlich > DR. Therefore, it can be assumed that the TP models are an accurate representation of the adsorption process. The maximum adsorption capacity estimated by the Langmuir isotherm is 167 mg/g, which is close to the experimental maximum of 153 mg/g. The accuracy of the models can be increased by using more and higher MB concentration data points.

3.11 Determination of thermodynamic parameters

The thermodynamic properties of the MB adsorption were identified. Using Eq. 16, the apparent equilibrium constant (K_c) was found. A linear line can be drawn, and the equilibrium constant is found from the gradient. Using the data in Fig. 14, a line was created for each temperature. This is seen in Fig. 17A, along with the trendline equations. The K_c value is 2.15, 0.63 and 0.6 for 30, 45 and 60 °C, respectively.

Using the equilibrium constant, the Gibbs free energy for each temperature can be calculated using Eq. 17. This was found to be -1,930, 1,202 and 1,426 J/mol for 30, 45 and 60 °C, respectively. Using the Gibbs free energy and temperature, the enthalpy and entropy of the MB adsorption can be found. A linear line can be created using Eq. 18. The line can be seen in Fig. 17B.

The gradient and intercept give the change in entropy and enthalpy, which was -112 J/mol K and -35 kJ/mol, respectively. Enthalpy between 2.1 and 20.9 kJ/mol indicates physical adsorption, while values between 80 and 200 kJ/mol indicate chemisorption [18]. Since enthalpy is negative, the adsorption process is exothermic, relying heavily on electrostatic interaction, hence why pH has a significant effect on adsorption [15, 18]. Because enthalpy and entropy are negative and Gibbs free energy is positive at 45 and 60 °C, the process is spontaneous at low temperatures and non-spontaneous at high temperatures [15, 18]. This trend was displayed in the thermodynamic study of other biosorbents [15, 18].

3.12 Comparison

The MB adsorption capacity of pea haulm was compared with other biosorbents recently studied in the literature. This comparison can be seen in Table 3. The table also displays adsorption conditions and matching kinetic and isotherm

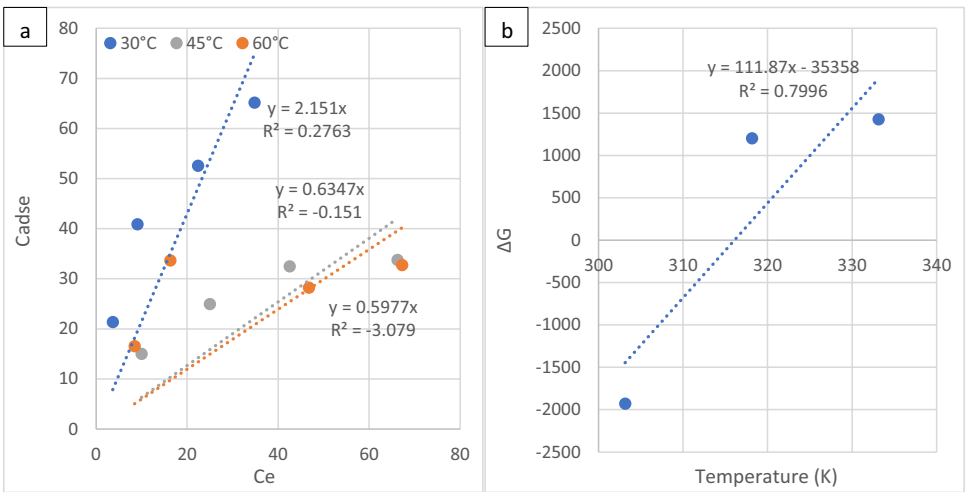

Fig. 17 **a** Thermodynamic equilibrium, **b**) enthalpy and entropy change.

Table 3 Comparison of biosorbents

Material	Adsorption Conditions	Adsorption capacity (mg/g)	Kinetics	Isotherm	Reference
Indian knotgrass	S: 200 D: 0.625 C: 750 A: 1200	426.39	Second-order	Langmuir	[14]
Brewer's spent grain	S: < 100 D: 1 C: 650 A: 650	284.75	Second-order	Freundlich	[15]
Edible fungi	S: D: 8 C: 350 A: 437.5	208.33	Second-order	Langmuir	[16]
Brazilian berry seeds	S: 35 D: 0.8 C: 200 A: 250	189.6	Second-order	Langmuir	[17]
Soybean hulls	S: 350 D: 1 C: 400 A: 400	169.9	Second-order	Langmuir	[18]
Pea haulm	S: ≤ 50 D: 0.5 C: 100 A: 200	167	Second-order	Temkin & Pyzhev	Present study
Indian almond	S: ≤ 36 D: 4 C: 800 A: 200	88.62	Second-order	Freundlich	[28]
wall barley	S: 100 D: 0.5 C: 100 A: 200	26.2	Second-order		[42]
Sugarcane Bagasse	S: 600 D: 2 C: 20 A: 10	9.41	Second-order	Sips	[39]
common lilac	S: D: 25 C: 25 A: 1	0.92	Second-order	Langmuir	[29]

models. With *S* being the particle size (μm), *D* being the biosorbent dosage (g/L), *C* being the MB concentration (mg/L) and *A* being the maximum possible MB adsorption (mg/g).

It can be seen that milled pea haulm is an effective MB adsorbent with a relatively high adsorption capacity and follows the same kinetic model as other biosorbents. In terms of RMSE value, the TP isotherm model was the best fit, which is different from other biosorbents. The Langmuir isotherm had the highest R^2 value, meaning it is still an applicable model.

It can be seen that the adsorption capacity is heavily influenced by particle size and available MB molecules. A low initial MB concentration and high adsorbent dosage will result in a low adsorption capacity. This is because there are too many unsaturated adsorption sites and not enough MB molecules to fill them. Smaller particle sizes will also increase the available adsorption sites per mass. These factors explain why some of the adsorption capacities are significantly lower. If these potential biosorbents underwent different experimental conditions, they might produce significantly higher adsorption capacities.

4 Conclusion

This study used pea haulm to remove MB from a dye mixture. SEM–EDX, FTIR and TGA were used to characterise the material. Characterisation revealed the surface to be coarse and heterogeneous and almost entirely made up of

carbon and oxygen. The presence of hydroxyl, carboxyl and aromatic functional groups was confirmed, which are useful for adsorption, and the composition of key biomass components was identified. To maximise the adsorption process, a small particle size of < 50 µm, a small dosage of 0.5 g/L, an alkaline solution, an agitation of 120 rpm and a lower temperature of 30 °C were preferred. Equilibrium was achieved in 4 h. Pseudo-second-order kinetics and the Temkin & Pyzhev isotherm were identified as the best fitting models for the biosorption process. But Langmuir and Freundlich also showed high goodness of fit. The maximum experimental adsorption capacity was 167 mg/g and the maximum theoretical adsorption capacity was 153 mg/g, higher than other materials considered good biosorbents. The thermodynamic study revealed that the biosorption process was exothermic and spontaneous at low temperatures. Compared with recent studies on biosorbents, the pea haulm is very promising, surpassing the adsorption capacity of some examples. Pea haulm is, therefore, a new and promising candidate for wastewater treatment. An alternative to activated carbon, having a lower cost, is widely available. This will be especially useful in newly industrialised countries dealing with high water pollution and requiring a quick, cheap and effective solution. Future work could include regeneration of pea haulm, the adsorption of other types of pollutants and economic analysis and comparison with activated carbon.

Author Contribution Mathew C. Holliday, Sharif H. Zein contributed to conceptualisation;

Mathew C. Holliday contributed to formal analysis, investigation, and writing—original draft preparation;

Daniel R. Parsons, Sharif H. Zein contributed to writing—review and editing;

Sharif H. Zein contributed to funding acquisition and supervision.

Funding This study was funded by the Teesside, Hull and York—Mobilising Bioeconomy Knowledge Exchange (THYME) ('RG-ENERGY-ZEIN-3278637-University of York') through Higher Education Funding Council for England (HEFCE).

Data availability The pea haulm was supplied by Brown & Co. and M. Meadley & Sons.

Declarations

Conflicting Interest The authors have no competing interests to declare that are relevant to the content of this article. All authors certify that they have no affiliations with or involvement in any organisation or entity with any financial interest or non-financial interest in the subject matter or materials discussed in this manuscript. The authors have no financial or proprietary interests in any material discussed in this article.

References

1. Crini G (2006) Non-conventional low-cost adsorbents for dye removal: A review. Bioresour Technol 97(9):1061–1085. https://doi.org/10.1016/j.biortech.2005.05.001
2. Geçgel Ü, Özcan G, Gürpınar GÇ (2013) Removal of Methylene Blue from Aqueous Solution by Activated Carbon Prepared from Pea Shells (*Pisum sativum*). J Chem 614083. https://doi.org/10.1155/2013/614083
3. Guo J-Z, Li B, Liu L, Lv K (2014) Removal of methylene blue from aqueous solutions by chemically modified bamboo. Chemosphere 111:225–231. https://doi.org/10.1016/j.chemosphere.2014.03.118
4. Guillot JD (2021) The impact of textile production and waste on the environment (infographic). https://www.europarl.europa.eu/pdfs/news/expert/2020/12/story/20201208STO93327/20201208STO93327_en.pdf. (Accessed 21/02/2022).
5. Elango G, Rathika G, Elango S (2017) Physico-Chemical Parameters of Textile Dyeing Effluent and Its Impacts with Casestudy. Int J Res Chem Environ 7(1):17–24
6. McMullan G, Meehan C, Conneely A, Kirby N, Robinson T, Nigam P, Banat I, Marchant R, Smyth W (2001) Microbial decolourisation and degradation of textile dyes. Appl Microbiol Biotechnol 56(1):81–87. https://doi.org/10.1007/s002530000587
7. Kant R (2012) Textile dyeing industry an environmental hazard. Nat Sci 4:22–26. https://doi.org/10.4236/ns.2012.41004
8. LaRose D (2017) To Dye For: Textile Processing's Global Impact,. https://www.carmenbusquets.com/journal/post/fashion-dye-pollution. (Accessed 21/02/2022).
9. Banat IM, Nigam P, Singh D, Marchant R (1996) Microbial decolorization of textile-dyecontaining effluents: A review. Bioresour Technol 58(3):217–227. https://doi.org/10.1016/S0960-8524(96)00113-7
10. Sayğılı H, Güzel F, Önal Y (2015) Conversion of grape industrial processing waste to activated carbon sorbent and its performance in cationic and anionic dyes adsorption. J Clean Prod 93:84–93. https://doi.org/10.1016/j.jclepro.2015.01.009
11. Wang H, Xie R, Zhang J, Zhao J (2018) Preparation and characterization of distillers' grain based activated carbon as low cost methylene blue adsorbent: Mass transfer and equilibrium modeling. Adv Powder Technol 29(1):27–35. https://doi.org/10.1016/j.apt.2017.09.027
12. Joshi M, Bansal R, Purwar R (2004) Colour removal from textile effluents. Indian J Fibre Text Res 29:239–259
13. Poots VJP, McKay G, Healy JJ (1976) The removal of acid dye from effluent using natural adsorbents—I peat. Water Res 10(12):1061–1066. https://doi.org/10.1016/0043-1354(76)90036-1
14. Alp Arici T (2021) Highly reusable plant-based biosorbent for the selective methylene blue biosorption from dye mixture in aqueous media. Int J Environ Sci Technol. https://doi.org/10.1007/s13762-021-03238-w
15. de Araújo TP, Tavares FO, Vareschini DT, Barros M (2020) Biosorption mechanisms of cationic and anionic dyes in a low-cost

residue from brewer's spent grain. Environ technol 42(19):1–16. https://doi.org/10.1080/09593330.2020.1718217
16. Bo L, Gao F, Shuangbao BY, Liu Z, Dai Y (2021) A novel adsorbent Auricularia Auricular for the removal of methylene blue from aqueous solution: Isotherm and kinetics studies. Environ Technol & Innov 23:101576. https://doi.org/10.1016/j.eti.2021.101576
17. Georgin J, Franco DSP, Netto MS, Allasia D, Oliveira MLS, Dotto GL (2020) Treatment of water containing methylene by biosorption using Brazilian berry seeds (Eugenia uniflora). Environ Sci Pollut Res 27(17):20831–20843. https://doi.org/10.1007/s11356-020-08496-8
18. Cusioli LF, Quesada HB, Baptista ATA, Gomes RG, Bergamasco R (2020) Soybean hulls as a low-cost biosorbent for removal of methylene blue contaminant. Environ Prog Sustain Energy 39(2):13328. https://doi.org/10.1002/ep.13328
19. Nimbalkar PR, Khedkar MA, Chavan PV, Bankar SB (2018) Biobutanol production using pea pod waste as substrate: Impact of drying on saccharification and fermentation. Renew Energy 117:520–529. https://doi.org/10.1016/j.renene.2017.10.079
20. Gao Y, Xia H, Sulaeman AP, de Melo EM, Dugmore TIJ, Matharu AS (2019) Defibrillated Celluloses via Dual Twin-Screw Extrusion and Microwave Hydrothermal Treatment of Spent Pea Biomass. ACS Sustain Chem Eng 7(13):11861–11871. https://doi.org/10.1021/acssuschemeng.9b02440
21. Verma N, Bansal MC, Kumar V (2011) Pea peel waste: A lignocellulosic waste and its utility in cellulase production by Trichoderma reesei under solid state cultivation. Bioresour 6(2):15
22. Dod R, Banerjee G, Saini S (2012) Adsorption of methylene blue using green pea peels (Pisum sativum): A cost-effective option for dye-based wastewater treatment. Biotechnol Bioprocess Eng 17(4):862–874. https://doi.org/10.1007/s12257-011-0614-5
23. Tharaneedhar V, Kumar PS, Saravanan A, Ravikumar C, Jaikumar V (2017) Prediction and interpretation of adsorption parameters for the sequestration of methylene blue dye from aqueous solution using microwave assisted corncob activated carbon. Sustain Mater Technol 11:1–11. https://doi.org/10.1016/j.susmat.2016.11.001
24. Ghosh D, Bhattacharyya KG (2002) Adsorption of methylene blue on kaolinite. Appl Clay Sci 20(6):295–300. https://doi.org/10.1016/S0169-1317(01)00081-3
25. Madduri S, Elsayed I, Hassan EB (2020) Novel oxone treated hydrochar for the removal of Pb(II) and methylene blue (MB) dye from aqueous solutions. Chemosphere 260:127683. https://doi.org/10.1016/j.chemosphere.2020.127683
26. Rzig B, Guesmi F, Sillanpää M, Hamrouni B (2021) Modelling and optimization of hexavalent chromium removal from aqueous solution by adsorption on low-cost agricultural waste biomass using response surface methodological approach. Water Sci Technol 84(3):552–575. https://doi.org/10.2166/wst.2021.233
27. Koyuncu H, Kul AR (2020) Removal of methylene blue dye from aqueous solution by nonliving lichen (Pseudevernia furfuracea (L) Zopf) as a novel biosorbent. Appl Water Sci 10:72. https://doi.org/10.1007/s13201-020-1156-9
28. Hevira L, Zilfa R, Ighalo JO, Aziz H, Zein R (2021) Terminalia catappa shell as low-cost biosorbent for the removal of methylene blue from aqueous solutions. J Ind Eng Chem 97:188–199. https://doi.org/10.1016/j.jiec.2021.01.028
29. Gulluce E, Karadayi M, Gulluce M, Karadayi G, Yildirim V, Egamberdieva D, Alaylar B (2020) Bioremoval of methylene blue from aqueous solutions by Syringa vulgaris L hull biomass. J Environ Sustain 3(3):303–312. https://doi.org/10.1007/s42398-020-00122-0
30. Lagergren S (1898) Zur theorie der sogenannten adsorption gelöster stoffe. Kongl Vetensk Acad Handl 24(4):1–39
31. Ho YS, McKay G (1998) Sorption of dye from aqueous solution by peat. Chem Eng J 70(2):115–124. https://doi.org/10.1016/S0923-0467(98)00076-1
32 Langmuir I (1916) The Constitution and Fundamental Properties of Solids and Liquids. Part I Solids J Am Chem Soc 38(11):2221–2295. https://doi.org/10.1021/ja02268a002
33. Hall KR, Eagleton LC, Acrivos A, Vermeulen T (1966) Pore- and Solid-Diffusion Kinetics in Fixed-Bed Adsorption under Constant-Pattern Conditions. Ind Eng Chem Fund 5(2):212–223. https://doi.org/10.1021/i160018a011
34. Freundlich HMF (1906) Über die Adsorption in Lösungen. Z Phys Chem 57(1):385–471
35. Temkin MI, Pyzhev V (1940) Kinetics of Ammonia synthesis on promoted Iron catalyst. Acta Physicochimica URSS 12:327–356
36. Dubinin M, Radushkevich LV (1947) The Equation of the Characteristic Curve of Activated Charcoal. Proc USSR Acad Sci 55:327–329
37. Bouras HH, Isik Z, Arikan EB, Yeddou AR, Bouras N, Chergui A, Favier L, Amrane A, Dizge N (2020) Biosorption characteristics of methylene blue dye by two fungal biomasses. Int J Environ Sci Technol 78(3):365–381. https://doi.org/10.1080/00207233.2020.1745573
38. Yang H, Yan R, Chen H, Lee DH, Zheng C (2007) Characteristics of hemicellulose, cellulose and lignin pyrolysis. Fuel 86(12):1781–1788. https://doi.org/10.1016/j.fuel.2006.12.013
39. Siqueira TCA, de Silva IZ, Rubio AJ, Bergamasco R, Gasparotto F, Paccola EAS, Yamaguchi NU (2020) Sugarcane Bagasse as an Efficient Biosorbent for Methylene Blue Removal: Kinetics, Isotherms and Thermodynamics. Int J Environ Res Public Health 17:526. https://doi.org/10.3390/ijerph17020526
40. Office of Air and Radiation (2003) Particle Pollution and your Health. United States Environmental Protection Agency. https://www.airnow.gov/sites/default/files/2018-03/pm-color.pdf [Accessed 21/02/2022]
41. Prabhasankar P, Rao PH (2001) Effect of different milling methods on chemical composition of whole wheat flour. Eur Food Res Technol 213(6):465–469. https://doi.org/10.1007/s002170100407
42. Al-Mahmoud S (2020) Kinetic and Thermodynamic Studies for the Efficient Removal of Methylene Blue Using Hordeum Murinum as a New Biosorbent. Egypt J Chem 63(9):3381–3390. https://doi.org/10.21608/ejchem.2020.16008.1970